

Possibilities and Limits of Axial Lifetime Control by Radiation Induced Centers in Fast Recovery Diodes

Ralf Siemieniec and Josef Lutz

AFFILIATIONS

Ralf Siemieniec, Technical University of Ilmenau, Department of Solid-State Electronics,
P.O. Box 100565, D-98684 Ilmenau, Germany, e-mail: ralf.siemieniec@tu-ilmenau.de

Josef Lutz, Chemnitz University of Technology, Faculty of Electrical Engineering and
Information Technology, D-09107 Chemnitz, Germany, e-mail: josef.lutz@infotech.tu-
chemnitz.de

KEYWORDS

lifetime control, irradiation, recombination, simulation, fast recovery diode, impatt
oscillation

ABSTRACT

Device simulation, based on an extended recombination model, is used as a design tool for lifetime-controlled power diodes with different lifetime profiles. Homogenous and local recombination center profiles are considered. The sensitivity of important device properties, such as the trade-off between stationary and dynamical characteristics, to the recombination center peak position is investigated. The occurrence of dynamic impatt oscillations is analyzed.

INTRODUCTION

The use of irradiation techniques for carrier lifetime control is nowadays a commonly accepted strategy for optimizing power device characteristics. In comparison with the conventionally used impurities gold and platinum, the irradiation techniques offer an exact process control and the possibility to realize different lifetime profiles. Today, irradiation-based lifetime adjustment steps are applied to a wide variety of power devices like IGBTs, GTOs and Freewheeling Diodes (FWDs).

The improvement and optimization of radiated devices was usually done through time- and cost-consuming experiments. Using a device simulation tool with an appropriate extended recombination model allows a significant reduction of the necessary experimental efforts. Based on center parameters determined in earlier work [13,14], the effects of different lifetime profiles on the stationary and dynamical characteristics of fast recovery diodes are studied in this work using 2D device simulation. The validity of the results is demonstrated by comparison with measurements taken on manufactured samples.

LIFETIME CONTROL

In this work, device simulation is used for the investigation of the influence of various lifetime profiles on the properties of fast silicon power diodes with a blocking voltage of 1.2kV. Table 1 gives an overview of the studied basic profile types. Additionally, the irradiation dose was varied in a dose range as given in table 1. All manufactured samples were annealed using identical conditions at a temperature of more than 300°C for one hour. The nominal current density of the devices is app. 170A/cm².

SIMULATION MODEL

Irradiation generates centers with different energy levels in the band gap of Silicon. Each level may act as an effective recombination center where the total recombination rate results from the emission and capture processes of each single level as illustrated in Figure 1. The implementation of this extended model, which includes the complete trap dynamics, is fundamental for an appropriate simulation of such devices [4,21].

For all simulations, the 2D device simulator TeSCA has been used [3]. This simulation system solves the three fundamental semiconductor equations (the Poisson equation as well as the electron and hole current continuity equation). For the consideration of deep traps, additional terms are necessary. In the Poisson equation (1), the charged recombination centers are considered. The thermal capture and emission processes of carriers via the deep levels within the band gap lead to additional recombination terms in the continuity equations (2) and (3). Here, the terms R and G refer to further recombination and generation mechanisms, such as auger recombination or avalanche. The occupancies of the acceptor and donor traps are evaluated from the balance equations (4) and (5) according to the relations of equations (6) and (7). The emission rates are calculated from the position of the recombination center within the band gap, the capture rates, the entropy factors and the temperature, as given in equations (8) to (11).

Based on this extended recombination model, the behavior of radiated devices is predicted with qualitatively and quantitatively good results [12,13,14].

RECOMBINATION CENTER DATA

Recombination Center Properties

For simulation purposes it is necessary not only to implement an appropriate recombination model but also to know the parameters of the radiation-induced centers as well as their temperature dependencies. Even though a lot of publications deal with recombination center parameter determination [1,5-7,18,22], reliable data were not available until recently due to the sophisticated and therefore fault sensitive character of the necessary measurements.

Table 2 shows the properties of the recombination-relevant centers, as used in the simulations, according to previous work [13,14]. There, the fundamental properties of the radiation-induced centers are determined by DLTS measurements [8]. Figure 2 shows, as an example, the majority and minority carrier DLTS spectrum measured at type E100. Due to the applied annealing step, the center E(90K) controls the high-level lifetime. Figure 3 gives the change of the calculated carrier lifetime under high-injection condition with the annealing of the acceptor-like radiation-induced centers.

Power devices are usually operated at high injection levels in on-state and turn-on/turn-off. Therefore, it is necessary to know the parameters of E(90K) exactly to allow correct simulations. Since the electron capture rate is small compared to the hole capture rate of E(90K), it is possible to use measurements of the high-level lifetime for an estimation of the temperature-dependent electron capture rate [14].

These measurements are based on the well-known OCVD (Open Circuit Voltage Decay) technique [9]. Due to the comparatively shallow energetic position of E(90K) within the band gap of silicon, optical excitation of carriers by means of laser light pulses was used to generate a large density of excess carriers to fulfill the high-injection condition [14].

The composition of the recombination centers detected in electron-radiated silicon depends on the irradiation parameters. Figure 4 shows the dependence of the trap density on electron energy and dose. In case of the lowest irradiation energy, E(230K) is not detectable. This recombination center is already vanished due to the annealing process. Under the applied conditions, the dependence of the generated centers is approximately linear to the irradiation dose.

Recombination Center Profile Estimation

DLTS measurements were also used for the determination of the concentration profiles in the helium-radiated samples. Due to the high concentrations, an additional second annealing step was necessary to allow the profile measurement of E(230K) to be performed.

Figure 5 shows the determined center distribution and the approximation based on a simple gaussian profile as used in the device simulations. For the traps H(195K) and E(90K), the same profile is assumed. The peak concentrations of these traps are estimated from the comparison of the results of lifetime measurements and measurements of the DLTS- and junction capacitance at the helium-radiated samples with and without an additional annealing step. Further work must improve the possibilities and the accuracy of recombination center profile measurement.

THE INFLUENCE OF LIFETIME CONTROL ON DEVICE PROPERTIES

Forward Characteristics

Figure 6 shows the forward characteristics of the different types E (electron irradiation), H (helium irradiation) and EH (combination of the electron irradiation of type E and the helium irradiation of type H) as a result of simulation and measurement. Beside a satisfying agreement between measurement and simulation results, figure 6 clearly indicates the influence of the different lifetime profiles on the forward voltage characteristics.

Figure 7 shows the impact of the temperature on the forward voltage at nominal current. This temperature dependency is strongly influenced by the properties of the recombination centers due to the temperature dependent capture rates of the dominant recombination center E(90K). The comparison of the measured and simulated characteristics of type E shows a good accordance. The deviations in case of the types H and EH are most probably caused by the uncertainties of the recombination center profile measurements. Due to the higher forward voltage drop in type EH, other effects, like self-heating caused by recombination heat, may cause an additional error.

Nevertheless, figure 7 shows the change in the temperature coefficient due to the different irradiation types. Therefore, lifetime control offers a chance to slightly tune the temperature coefficient. This is important since a positive temperature coefficient simplifies the paralleling of power devices.

In difference to results recently published by other authors, as in [20], no further adjustment of recombination center parameters, especially the capture rates of the dominant center E(90K), was needed due to the sophisticated measurement techniques used [14].

Turn-Off Characteristics

Figure 8 gives a comparison of the reverse recovery current peak I_{RRM} for the different types E, H and EH. Figure 9 shows the comparison of the stored charge Q_{RR} . As in case of the forward voltage dependencies, these figures give clear evidence to the effects of the different irradiation processes. Obviously, type EH offers the best properties with respect to a low reverse recovery current peak I_{RRM} and the lowest stored charge Q_{RR} .

In case of type H deviations between measurement and simulation are caused by a larger tail current in the measurement compared to the simulation, and by non-calibrating the simulation parameters of the avalanche generation model.

Under common operating conditions, a sinusoidal current lower than the nominal current is often switched in usual topologies. Due to the reduced number of stored carriers in the low-doped region of the freewheeling diode, this is a critical condition for the device. As an example of type E, shown in figure 10, low current may cause a snap-off in the reverse current. This leads to overvoltages and/or oscillations due to parasitic inductances. The use of device simulation offers an opportunity for an optimization of the device design to avoid such a behavior.

The Influence of Recombination Center Peak Position

As commonly known, the combination of local and homogenous lifetime control is one possibility to realize fast FWDs with soft recovery behavior and a high dynamical ruggedness [10]. If local lifetime adjustment is applied, the peak position x_p-x_j of the recombination center profile, as illustrated in figure 11, controls the trade-off between forward losses and the stored charge as well as the trade-off between forward losses and reverse recovery current maximum. In this investigation, the peak position of a constant recombination center profile was moved

along the vertical axis, while homogenous base lifetime has been reduced as in case of an applied electron irradiation. Figure 12 shows the trade-off between forward voltage drop and the reverse recovery current maximum while figure 13 shows the trade-off between forward losses and the stored charge, both in dependence of the recombination center peak position, as a result of device simulation. A minimum is found at a recombination center peak position close to the pn-junction for both dependencies.

Dynamic Effects

Furthermore, device simulation holds potential to avoid disturbing dynamic effects. As an example, figure 14 shows the reverse recovery measurement of type E45, where impatt (impact ionization transit-time) oscillations appear. The measurement was done using a conventional double-pulse method.

The oscillations are caused by the temporarily positively-charged donors H(195K) which enhance the effective doping and therefore reduce the reverse blocking capability. Consequently, avalanche breakdown occurs at the pn-junction region and generates electrons. These electrons counterbalance the positive donors and hence stop the avalanche generation of carriers. Due to the electric field, the electrons are transported to the nn^+ -junction and again, avalanche generation starts at the pn-junction. The impatt oscillations stop as soon as the positive donors are discharged and the device is again able to withstand the reverse voltage [11]. The frequency of the oscillations depends on the transit-time of the electron carrier flow through the low-doped region of the device. Thus, the oscillation frequency is defined by the carrier saturation velocity v_d , depending on the strength of the electric field, and the width of the low-doped region w_B (equation 12).

For simulation purposes, we use an emulation of the measurement setup. The simulation circuit consists of the discrete freewheeling diode, a time-variable serial resistance instead of the IGBT and a small inductance. This emulation was used to decrease the necessary computing time since only the diode has to be considered.

Figure 15 shows a simulation of type E45 (electron dose $d=1\cdot 10^{15}\text{ cm}^{-2}$) where impatt oscillations are observed. Figure 16 shows the electron carrier distribution at different points in time as a result of device simulation, while figure 17 shows the change of the electrical field with time to exemplify the physical processes in the device.

The avoidance of these high-frequency oscillations is necessary because of their adverse influence on drive control units and because of EMC (electromagnetic compatibility) issues. According to previous work [11], the threshold voltage of the impatt oscillation mainly depends on the concentration of the donor-state H(195K), the reverse voltage and the temperature.

Figure 18 shows the threshold voltage V_{DI} of type E45 in dependence of temperature for different irradiation doses. The measured values from [11] are compared with the simulation results. The agreement is sufficient. Additionally, an analytical estimation arrives from the discharging of the centers H(195K) due to the thermal emission of previously captured holes as described in detail in [11]. Figure 18 also includes the results of this estimation, based on an abrupt pn-junction, the ionization coefficients published in [2,16] with the temperature dependency given in [17] and a triangular-shaped electrical field (as shown in figure 17).

Obviously, the temperature dependency of the threshold voltage of impatt oscillation can be predicted using simulation. Thus, Figure 18 indicates the potential of device simulation if deep centers are considered.

CONCLUSION

To consider lifetime killing effects in device simulation, the use of an extended recombination model including full trap dynamics is necessary. The introduction of several recombination centers with different properties into simulation allows the correct description of recombination processes under different conditions.

The previously determined center parameters, which were used for the simulations in this work, explain the temperature dependencies of stationary and dynamic characteristics. Based on these results, device simulation is used as a tool for device design. The influence of different recombination center profiles on the stationary and dynamic properties of freewheeling diodes is studied.

It is shown that for the realization of a fast and soft freewheeling diode, the optimal position of the recombination center peak is located close to the pn-junction which is in agreement with previously published results [10,15,19].

Furthermore, the physically correct description of the trap dynamics allows an appropriate simulation of dynamic impatt oscillations. This effect is caused by temporarily positively-charged donor-states which reduce the blocking capability of the device. The consideration of the donor-states is necessary in case of high-dose electron, proton or helium ion irradiation to prevent high-frequency oscillations. Consequently, the use of high-energy particles for carrier lifetime control is limited due to the formation of these unavoidable defects.

Therefore, device simulation may be used as a powerful tool in the development and optimization of power devices as well as in the explanation of their behavior.

ACKNOWLEDGEMENTS

The authors wish to thank the scientists, especially Dr. Nürnberg and Prof. Gajewski, from the Weierstrass Institute for Applied Analysis and Stochastics in Berlin, who developed the device simulator TeSCA. Moreover, the authors are grateful for their support and the addition of new features and algorithms into the simulation system.

The Authors would like to thank also Ms. Pellkofer and Mr. Umland for their support in sample preparation and measurement assistance.

We also wish to thank Prof. Wagemann from the Technical University of Berlin for the opportunity to perform DLTS measurements.

This work has been supported by grants of the Deutsche Forschungsgemeinschaft.

REFERENCES

- [1] Bleichner, H., Jonsson, P. and Keskitalo, N.: Temperature and injection dependence of the Shockley-Read-Hall-lifetime in electron irradiated n-type silicon, *Journal of Applied Physics*, 79(12), 1996, 9142-9148
- [2] Fulop, W.: Calculations of Avalanche Breakdown Voltages of Silicon pn-Junctions, *Solid-State Electronics*, 10, 1967, 39-42
- [3] Gajewski, H., Heinemann, B. and Langmach, H.: *TeSCA-Handbuch*, Weierstrass-Institute for Applied Analysis and Stochastics Berlin, 1991
- [4] Hazdra, P. and Vobecký, J.: Accurate Simulation of Fast Ion Irradiated Power Devices, *Solid-State Electronics*, 37(1), 1994, 127-134
- [5] Hüppi, M. W.: *Protonenbestrahlung von Silizium: Vollständige elektrische Charakterisierung der erzeugten Rekombinationszentren*, Dissertation ETH Zürich, 1989
- [6] Irscher, K.: *Kapazitätsspektroskopische Analyse tiefer Störstellen in ionenimplantiertem Silizium*, Dissertation Humboldt-University of Berlin, 1985
- [7] Keskitalo, N.: *Irradiation Induced Defects for Lifetime Control in Silicon*, Dissertation Uppsala University, 1997

- [8] Lang, D.V.: Deep-Level Transient Spectroscopy: A New Method to Characterize Traps in Semiconductors, *Journal of Applied Physics*, 45(7), 1974, 3023-3032
- [9] Lederhandler, S.R. and Giacoletto, L.J.: Measurement of Minority Carrier Lifetime and Surface Effects in Junction Devices, *Proc. IRE* (1955), 477-483
- [10] Lutz, J.: Axial Recombination Centre Technology for Freewheeling Diodes, *Proc. EPE*, 1502-1506, 1997 (Trondheim 1997)
- [11] Lutz, J., Südkamp, W. and Gerlach, W.: Impatt Oscillations in Fast Recovery Diodes due to Temporarily Charged Radiation-Induced Deep Levels, *Solid-State Electronics*, 42(6), 1998, 931-938
- [12] Siemieniec, R., Südkamp, W. and Lutz, J.: Simulation and Experimental Results of Radiation Induced Traps in Silicon, *Proc. EPE'99* (Lausanne 1999)
- [13] Siemieniec, R., Südkamp, W. and Lutz, J.: Applying Device Simulation for Lifetime-Controlled Devices", *Proc. ICCDCS 2002* (Aruba 2002)
- [14] Siemieniec, R., Südkamp, W. and Lutz, J.: Determination of Parameters of Radiation Induced Traps in Silicon, *Solid-State Electronics*, 46(6), 2002, 891-901
- [15] Silber, D., Nowak, W.D., Wondrak, W., Thomas, B., Berg, H.: Improved Dynamic Properties of GTO-Thyristors and Diodes by Proton Implantation, *IEDM*, 1985, 162-165

- [16] Shields, J.: Breakdown in Silicon pn-Junctions, Journ. Electron. Control, 6, 1959
- [17] Singh, R., Baliga, B.J.: Analysis and optimization of power MOSFETs for cryogenic operation, Solid-State Electronics, 36(8), 1993, 1203-1211
- [18] Südkamp, W.: *DLTS-Untersuchung an tiefen Störstellen zur Einstellung der Trägerlebensdauer in Si-Leistungselementen*, Dissertation Technical University of Berlin, 1994
- [19] Vobecký, J., Hazdra, P., Homola, J.: Optimization of Power Diode Characteristics by Means of Ion Irradiation, IEEE Trans. Electron Devices, Vol. ED-43 (12), 1996, 2283-2289
- [20] Vobecký, J., Hazdra, P., Humbel, O., Galster, N.: Crossing point current of electron and proton irradiated power P-i-N diodes, Microelectronics Reliability, 40, 2000, 427-433
- [21] Wertheim, G.K.: Transient Recombination of Excess Carriers in Semiconductors, Physical Review, 100(4), 1958, 1086-1091
- [22] Wondrak, W.: *Erzeugung von Strahlenschäden in Silizium durch hochenergetische Elektronen und Protonen*, Dissertation University Frankfurt/M., 1985

FIGURES

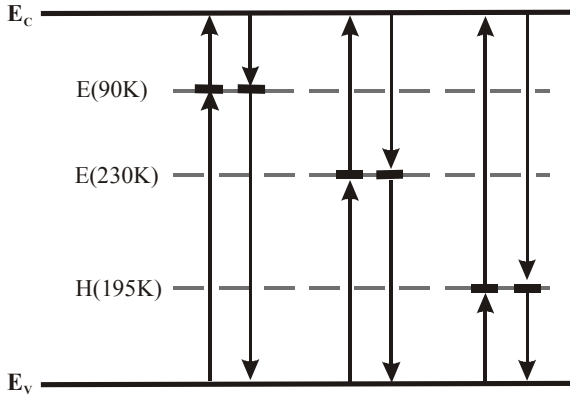


Figure 1: Recombination via independent centers

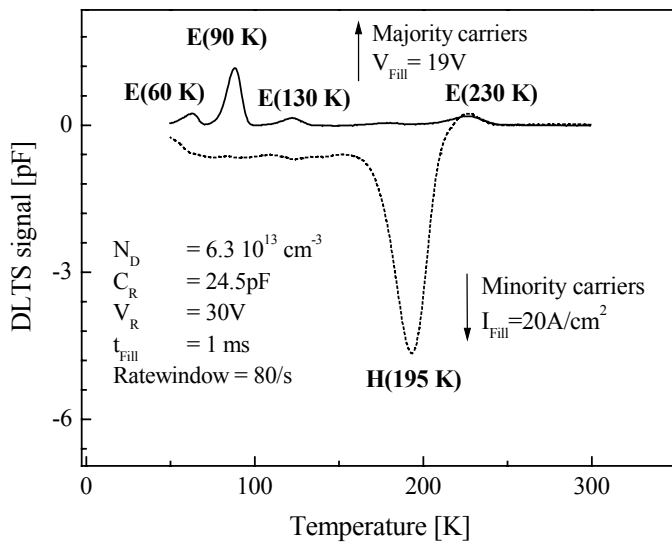


Figure 2: DLTS spectrum of measurement at type E100 ($d=1.1 \cdot 10^{14} \text{ cm}^{-2}$)

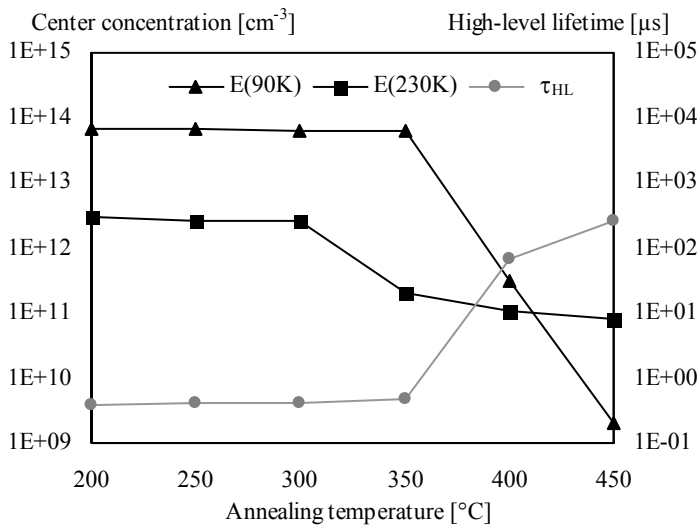


Figure 3: Annealing of radiation-induced acceptors in electron-radiated silicon (data from [22])

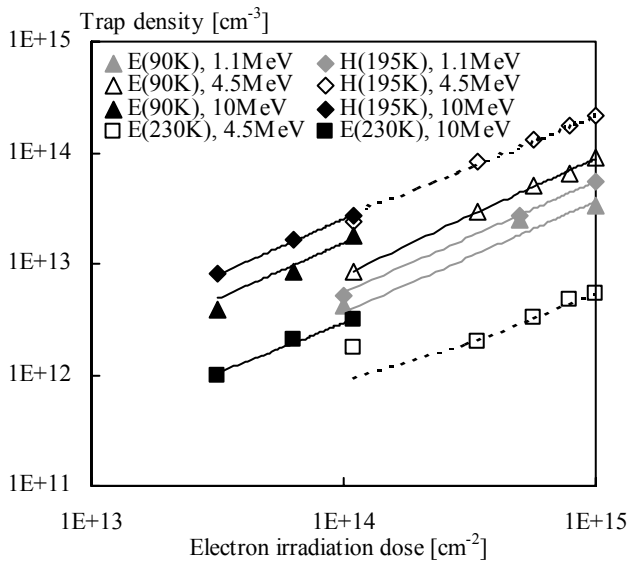


Figure 4: Trap density vs. parameters of electron irradiation

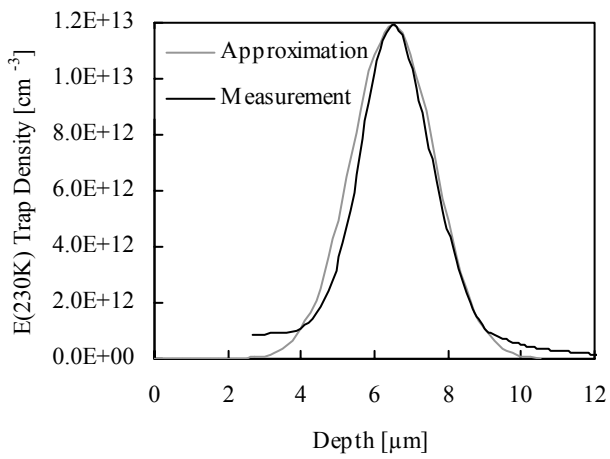


Figure 5: Recombination center profile of E(230K) after additional annealing of type H ($d=7 \cdot 10^{10} \text{ cm}^{-2}$)

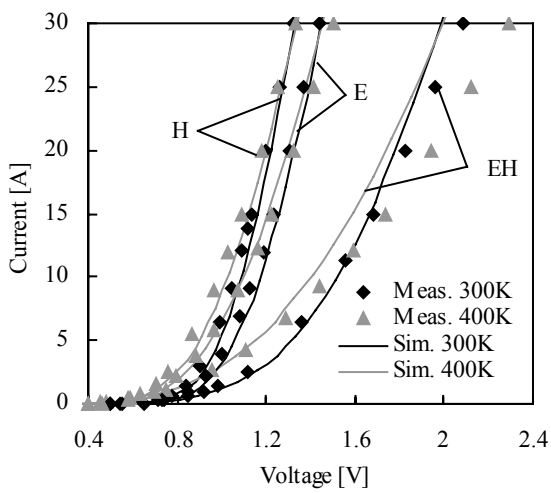


Figure 6: Forward characteristics of types H ($d=7 \cdot 10^{11} \text{ cm}^{-2}$), E ($d=1 \cdot 10^{15} \text{ cm}^{-2}$) and EH

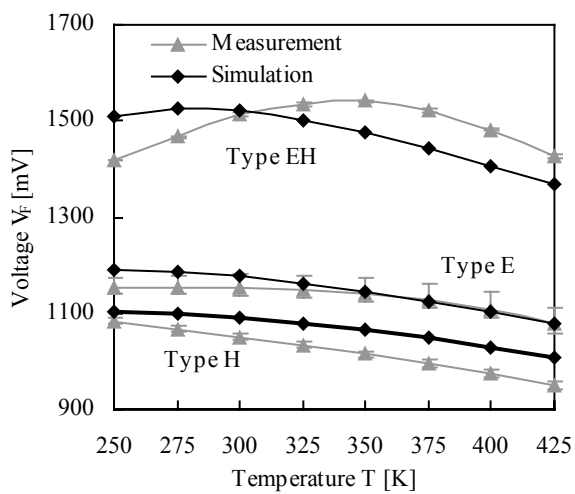


Figure 7: Forward voltage dependence on temperature ($I_F=10A$) of types H ($d=7 \cdot 10^{11} \text{ cm}^{-2}$), E ($d=1 \cdot 10^{15} \text{ cm}^{-2}$) and EH

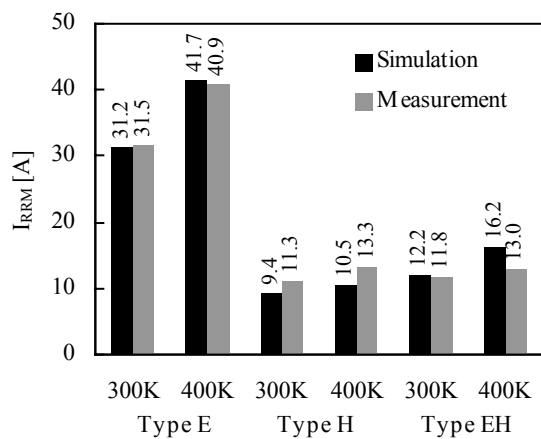


Figure 8: I_{RRM} comparison ($V_R=250V$, $I_F=10A$, $di/dt=500A/\mu s$) of types H ($d=7 \cdot 10^{11} \text{ cm}^{-2}$), E ($d=1 \cdot 10^{15} \text{ cm}^{-2}$) and EH

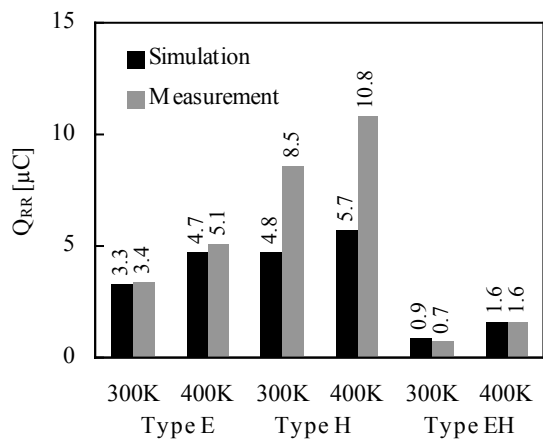


Figure 9: Q_{RR} comparison ($V_R=250V$, $I_F=10A$, $di/dt=500A/\mu s$) of types H ($d=7 \cdot 10^{11} \text{ cm}^{-2}$), E ($d=1 \cdot 10^{15} \text{ cm}^{-2}$) and EH

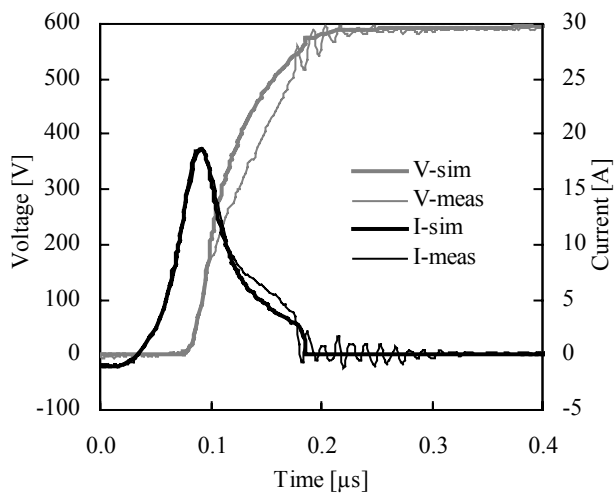


Figure 10: Snap-Off in reverse recovery of type E ($d=1 \cdot 10^{15} \text{ cm}^{-2}$) at low current ($V_R=600V$, $I_F=1A$, $di/dt=500A/\mu s$)

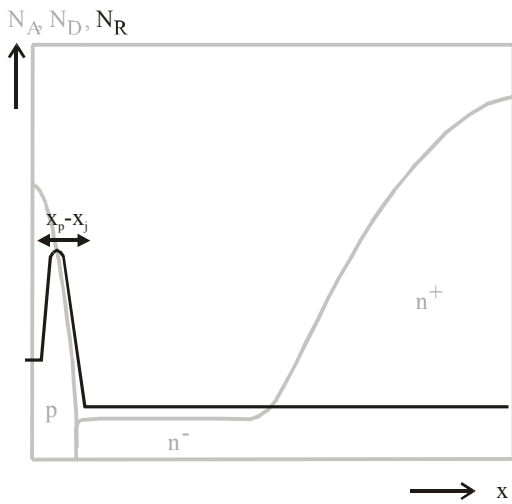


Figure 11: Doping and schematic recombination center profile

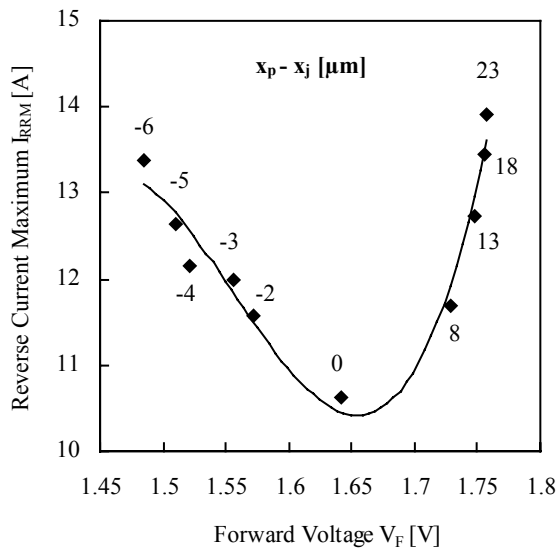


Figure 12: Trade-off between the forward voltage drop and the reverse recovery current maximum in dependence of the recombination center peak position, type EH

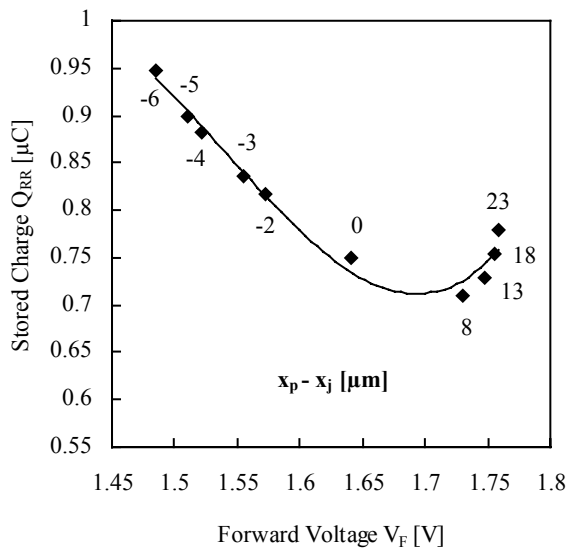


Figure 13: Trade-off between the forward voltage drop and the stored charge in dependence of the recombination center peak position, type EH

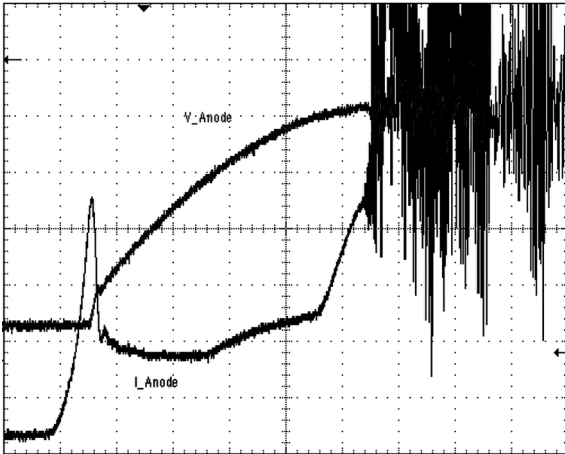


Figure 14: Oscillogram of temporary impatt oscillation at type E45, $d=1 \cdot 10^{15} \text{ cm}^{-2}$, $T=275\text{K}$, $V_R=790\text{V}$, $I_F=7\text{A}$ (5A/div, 200V/div, 200ns)

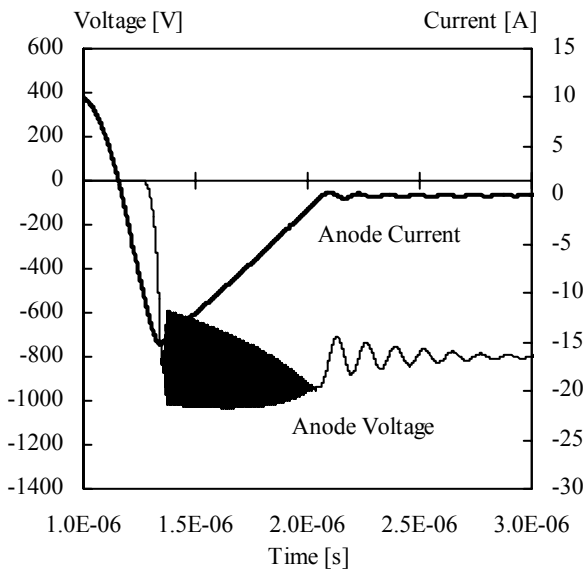


Figure 15: Simulation of temporary impatt oscillation at type E45, $d=1 \cdot 10^{15} \text{ cm}^{-2}$ ($T=300\text{K}$, $V_R=800\text{V}$, $I_F=10\text{A}$)

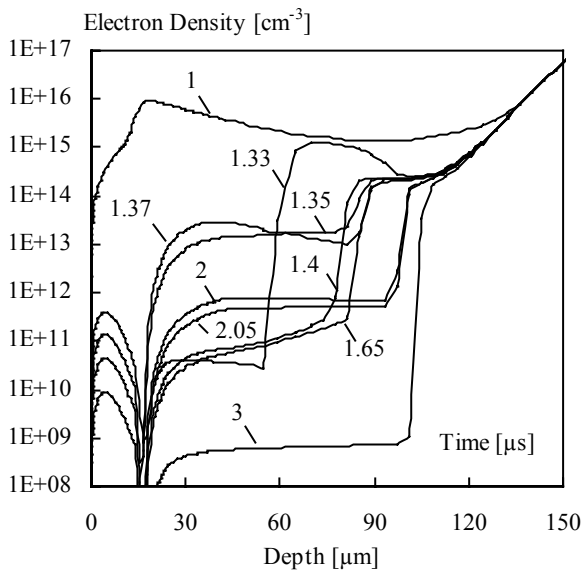


Figure 16: Electron distribution for different points in time during impatt oscillation at type E45, $d=1 \cdot 10^{15} \text{ cm}^{-2}$ ($T=300\text{K}$, $V_R=800\text{V}$, $I_F=10\text{A}$)

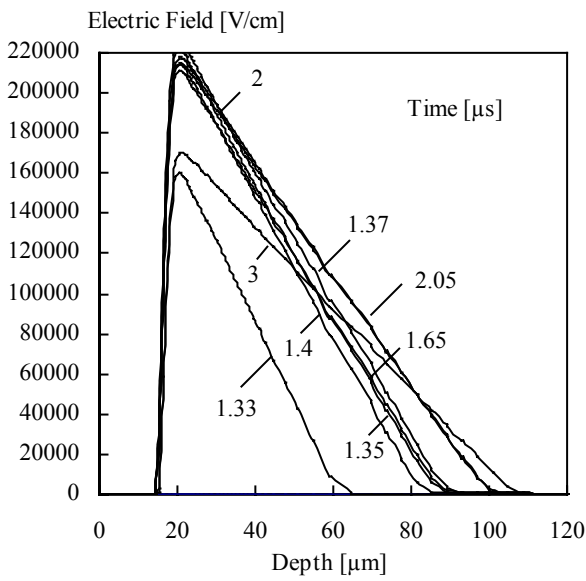


Figure 17: Electric field vs. time along vertical axis for different points in time during impatt oscillation at type E45, $d=1 \cdot 10^{15} \text{ cm}^{-2}$ ($T=300\text{K}$, $V_R=800\text{V}$, $I_F=10\text{A}$)

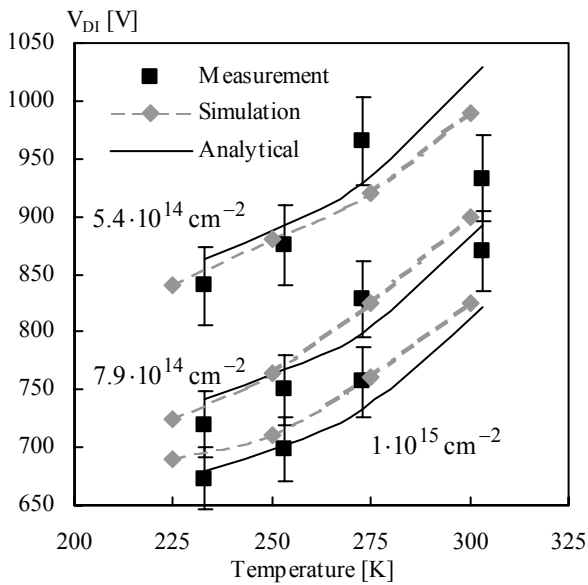


Figure 18: Threshold voltage of impatt oscillation for 4.5MeV electron-radiated devices. Measured and analytical values taken from [11]

TABLES

| Type | Profile | Particles | Particle Energy | Doses |
|------|----------------|---------------|-----------------|--|
| N | none | - | - | |
| H | local | helium ions | 5.4MeV | $7 \cdot 10^{10} \dots 7 \cdot 10^{11} \text{ cm}^{-2}$ |
| E | homogenous | electrons | 1.1MeV | $1 \cdot 10^{14} \dots 1 \cdot 10^{15} \text{ cm}^{-2}$ |
| E45 | homogenous | electrons | 4.5MeV | $1.1 \cdot 10^{14} \dots 1 \cdot 10^{15} \text{ cm}^{-2}$ |
| E100 | homogenous | electrons | 10MeV | $3.15 \cdot 10^{13} \dots 1.1 \cdot 10^{14} \text{ cm}^{-2}$ |
| EH | homogenous and | electrons and | 1.1MeV | $1 \cdot 10^{15} \text{ cm}^{-2}$ |
| | local | helium ions | 5.4MeV | $7 \cdot 10^{11} \text{ cm}^{-2}$ |

Table 1: Overview of studied profile types

| Trap | Energy level | Capture coefficients | |
|---------|--------------------------------|--|---|
| | | $c_n [\text{cm}^3/\text{s}]$ | $c_p [\text{cm}^3/\text{s}]$ |
| E(90K) | $E_C - E_T = 0.167 \text{ eV}$ | $1.15 \cdot 10^{-7} \exp\left(-\frac{T}{355.4\text{K}}\right)$ | $6.39 \cdot 10^{-7} \sqrt{\frac{T}{300}} \exp\left(\frac{6.15 \cdot 10^{-3}}{k_B T}\right)$ |
| E(230K) | $E_C - E_T = 0.447 \text{ eV}$ | $3.41 \cdot 10^{-8} \sqrt{\frac{T}{300}} \exp\left(\frac{22.13 \cdot 10^{-3}}{k_B T}\right)$ | $2.79 \cdot 10^{-8} \sqrt{\frac{T}{300}} \exp\left(-\frac{22.13 \cdot 10^{-3}}{k_B T}\right)$ |
| H(195K) | $E_T - E_V = 0.351 \text{ eV}$ | $9.85 \cdot 10^{-9} \sqrt{\frac{T}{300}} \exp\left(-\frac{85 \cdot 10^{-3}}{k_B T}\right)$ | $4.3 \cdot 10^{-9} \sqrt{\frac{T}{300}}$ |

Table 2: Recombination center properties

EQUATIONS

$$-\operatorname{div}(\varepsilon \cdot \operatorname{grad}\varphi) = q \left[p - n - N_A^- + N_D^+ + \Sigma \left(N_{TD}^+ - N_{TA}^- \right) \right] \quad (1)$$

$$\begin{aligned} \frac{\partial n}{\partial t} - \frac{1}{q} \operatorname{div} J_n = G - R + \Sigma \left[e_{nA} N_{TA}^- - c_{nA} n \left(N_{TA} - N_{TA}^- \right) \right] \\ + \Sigma \left[e_{nD} \left(N_{TD} - N_{TD}^+ \right) - c_{nD} n N_{TD}^+ \right] \end{aligned} \quad (2)$$

$$\begin{aligned} \frac{\partial p}{\partial t} + \frac{1}{q} \operatorname{div} J_p = G - R + \Sigma \left[e_{pA} \left(N_{TA} - N_{TA}^- \right) - c_{pA} p N_{TA}^- \right] \\ + \Sigma \left[e_{pD} N_{TD}^+ - c_{pD} p \left(N_{TD} - N_{TD}^+ \right) \right] \end{aligned} \quad (3)$$

$$\frac{df_A}{dt} = (c_{nA} n + e_{pA}) (1 - f_A) - (c_{pA} p + e_{nA}) f_A \quad (4)$$

$$\frac{df_D}{dt} = (c_{pD} p + e_{nD}) (1 - f_D) - (c_{nD} n + e_{pD}) f_D \quad (5)$$

$$N_{TA}^- = N_{TA} \cdot f_A \quad (6)$$

$$N_{TD}^+ = N_{TD} \cdot f_D \quad (7)$$

$$e_{nA} = \chi_{nA} c_{nA} n_i \exp\left(\frac{E_{TA} - E_i}{k_B T}\right) \quad (8)$$

$$e_{pA} = \chi_{pA} c_{pA} n_i \exp\left(\frac{E_i - E_{TA}}{k_B T}\right) \quad (9)$$

$$e_{nD} = \chi_{nD} c_{nD} n_i \exp\left(\frac{E_{TD} - E_i}{k_B T}\right) \quad (10)$$

$$e_{pD} = \chi_{pD} c_{pD} n_i \exp\left(\frac{E_i - E_{TD}}{k_B T}\right) \quad (11)$$

$$f \approx \frac{v_d}{w_B} \quad (12)$$

SYMBOLS

| | | | |
|---------------|---|-------------|---------------------------------------|
| p | hole concentration | G | generation rate |
| n | electron concentration | R | recombination rate |
| J_n | electron current density | J_p | hole current density |
| N_A | acceptor density | N_D | donor density |
| N_A^- | ionized acceptor density | N_D^+ | ionized donor density |
| N_{TA} | acceptor trap density | N_{TA}^- | ionized acceptor trap density |
| N_{TD} | donor trap density | N_{TD}^+ | ionized donor trap density |
| ε | permittivity | E_T | trap energy level |
| E_{TA} | acceptor trap energy level | E_{TD} | donor trap energy level |
| f_A | fraction of occupied acceptor traps | f_D | fraction of occupied donor traps |
| n_i | intrinsic density | E_i | intrinsic energy level |
| c_{nA} | electron capture rate of acceptor traps | c_{pA} | hole capture rate of acceptor traps |
| c_{nD} | electron capture rate of donor traps | c_{pD} | hole capture rate of donor traps |
| e_{nA} | electron emission rate of acceptor traps | e_{pA} | hole emission rate of acceptor traps |
| e_{nD} | electron emission rate of donor traps | e_{pD} | hole emission rate of donor traps |
| χ_{nA} | electron entropy factor of acceptor traps | χ_{pA} | hole entropy factor of acceptor traps |
| χ_{nD} | electron entropy factor of donor traps | χ_{pD} | hole entropy factor of donor traps |
| k_B | Boltzmann's constant | q | elemental charge |